JOC The Journal of Organic Chemistry

Article

pubs.acs.org/joc

Bent *N*-Heteroarenes

Sebastian Hahn, Florian L. Geyer, Silke Koser, Olena Tverskoy, Frank Rominger, and Uwe H. F. Bunz*

Organisch-Chemisches Institut, Ruprecht-Karls-Universität Heidelberg, Im Neuenheimer Feld 270, 69120 Heidelberg, Germany

Supporting Information

ABSTRACT: The syntheses and optical, electronic, and structural properties of a series of bent *N*-heteroarenes are described. The targets were obtained by condensation reactions of substituted aromatic *o*-diamines with 1,2-naphthoquinone and 1,2-anthraquinone in yields between 34 and 94%; naphthoquione-based products are generally formed in higher yields.

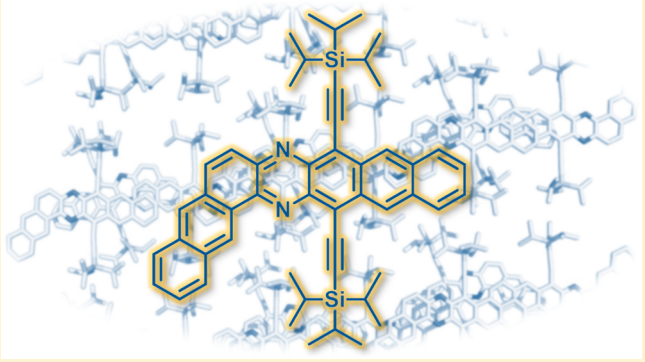

INTRODUCTION

We disclose full details of the syntheses of bent *N*-heteroarenes bearing azatetracene and azapentacene substructures[1] and discuss the influence of the attached bent part on the electronic, morphological, and structural properties of these materials. The synthesis and property evaluation of *N*-heteroacenes and *N*-heteroarenes is an attractive proposition, as the field of acenes experienced a second spring since the discovery of the superb semiconducting properties of pentacene, rubrene, and their relatives. Attachment of solubilizing and stabilizing substituents[2] has furthermore increased the level of interest in acenes.[3] This development was fueled by the work of Scott[4] and Müllen,[5] who prepared large and very large aromatic hydrocarbons.

For heteroacenes, which ironically have been known longer than most of the larger acenes,[6] a rekindling of interest has taken longer.[7] The report of Miao et al. that the symmetrical tetraazapentacene (TIPS-TAP)[8] is a high-performing n-channel semiconductor[9] further pointed interest toward *N*-heteroacenes and *N*-heteroarenes in general.[10] While different types of syntheses have been developed,[11] often the classic condensations of diketones or quinones with *ortho*-substituted aromatic diamines remain the most effective. That is particularly the case if the formed target is not a linear *N*-heteroacene (i.e., consists of only linearly annulated six-membered rings) but contains other structural elements such as four-membered rings or triptycene units.[12] In this study, we present the syntheses and optical and structural properties of bent azaheterocycles that form in good to excellent yields.

Bent *N*-heteroarenes are of great potential interest as emitting materials in organic light-emitting diodes (OLED), but also, larger bent *N*-heteroarenes should be useful as electron-injecting layers in OLEDs; the larger bent *N*-heteroarenes could be equally attractive both as charge transport materials in organic field effect transistors and, if one creates amorphous derivatives, as *N*-semiconductors for use in organic photovoltaic applications.

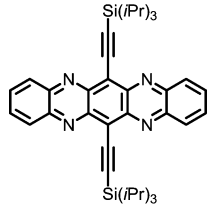

TIPS-TAP

RESULTS AND DISCUSSION

Synthesis. Scheme 1 depicts the modular synthetic approach to our targets. We reacted five different aromatic *o*-diamines with three different *o*-diketones. From Scheme 1, we glean that the reactions with 1,2-naphthalenedione **6** give the highest yield, followed by the indanedione **5**, and the lowest yields are obtained by condensation reactions of **7** with anthracenedione **4**. Even the lowest-yield reaction, the formation of **2e**, proceeds with 34% yield. Typical yields range between 50 and 70% after crystallization and chromatography. In some cases (as indicated in Scheme 1), the dihydro compound forms as a side product, which we did not separate but directly oxidized into the target, using MnO_2. This modular approach is flexible and furnishes 14 bent *N*-heteroarenes (**1a**−**e**, **2a**−**e**, and **3a**−**d**) easily and with reasonable to excellent yields.

Optical Properties. Figure 1 shows the absorption and emission of **1a**−**e** under daylight and illumination at 365 nm, while Figures 2 and 3 depict their UV−vis spectra in solution and in the solid state. Table 1 summarizes their optical properties in

Received: July 10, 2016
Published: August 19, 2016

DOI: 10.1021/acs.joc.6b01654
J. Org. Chem. 2016, 81, 8485−8494

Scheme 1. Synthesis of the Diaza- and Tetraazaheteroarenes 1a–3e by Condensation of 7a–e to 1,2-Naphthalenedione 6, 1,2-Anthracenedione 4, and 1,2-Indanedione 5

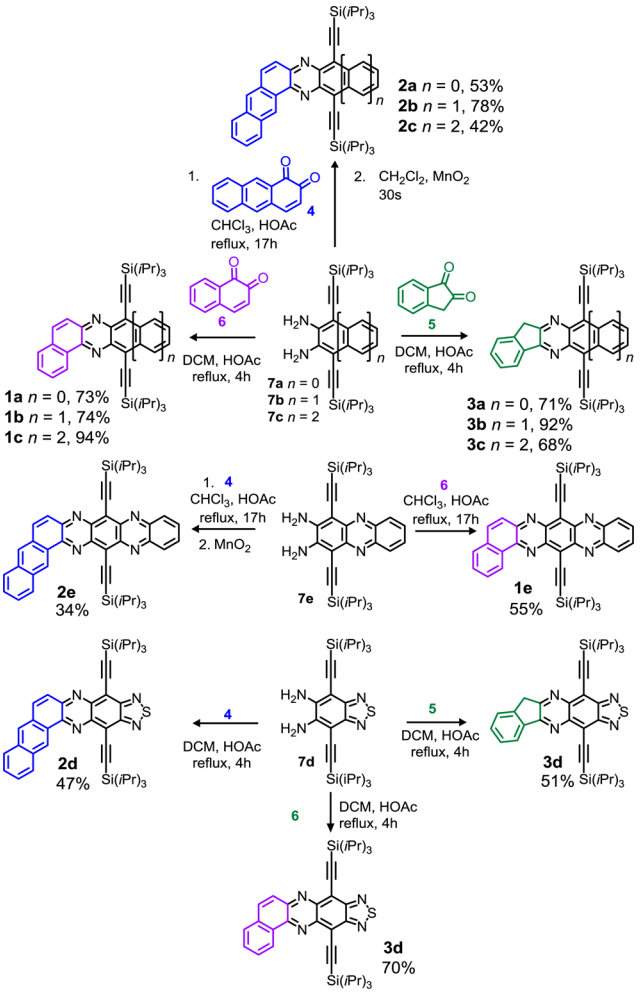

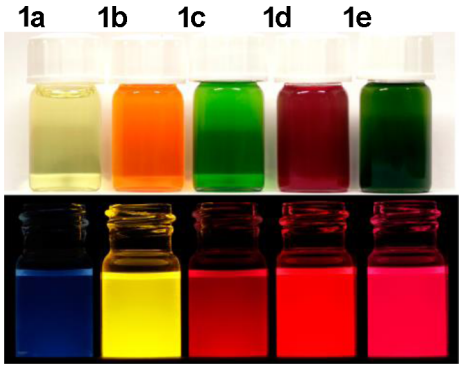

Figure 1. Photographs of **1a–e** (from left to right, respectively) in daylight (top) and under black light with illumination at 365 nm (bottom) in *n*-hexane.

solution. A significant red shift of the UV–vis spectra of **1a–e** is observed changing from the solution to solid state, accompanied by loss of the materials' fluorescence. **1b** and **3d** exhibit strong fluorescence with Φ values of 51 and 52%, respectively, in *n*-hexane. Interestingly, compounds **1b–d** show fluorescence higher than those of their larger analogues, **2b–d**, and the fluorescence of **1e** and **2e** is similar.

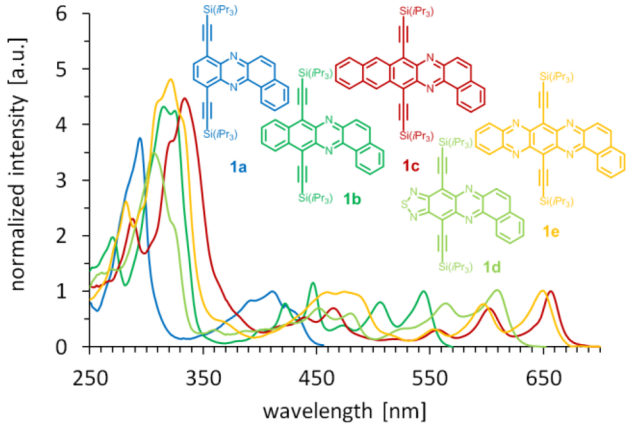

Figure 2. Normalized (lowest-energy maximum) absorption spectra of **1a–e** in *n*-hexane. The emission spectra of **1a–e** are shown in the Supporting Information.

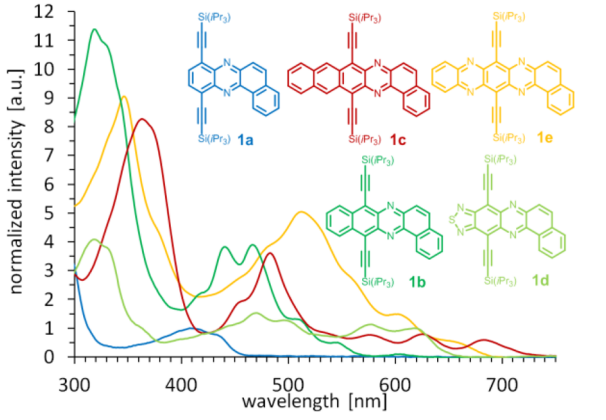

Figure 3. Normalized (lowest-energy maximum) thin-film absorption spectra of **1a–e**. The red shift observed upon the transition from solution to the solid state is 20 nm for **1a**, 4 nm for **1b**, 26 nm for **1c**, 13 nm for **1d**, and 10 nm for **1e**.

Table 1. Photophysical Properties of 1a–e, 2a–e, 3a–d, 8, 9, and TIPS-TAP in Solution (*n*-hexane)[a]

compd	$\lambda_{max\ abs}$ (nm)	λ_{onset} (nm)	$\lambda_{max\ em}$ (nm)	Stokes shift (nm)	ε (L M^{-1} cm^{-1})	Φ^f
TIPS-TAP	681	718	694	13	–	–
1a	411	446	444	33	46377	0.05
1b	544	558	553	9	36918	0.51
1c	656	670	661	5	29789	0.22
1d	607	631	617	10	46989	0.42
1e	649	667	656	7	20685	0.23
2a	463	471	466	3	24419	0.37
2b	536	558	548	12	13631	0.12
2c	644	670	654	10	28270	0.26
2d	579	626	605	26	44173	0.13
2e	638	655	648	10	10836	0.25
3a	369	407	430	61	8640	0.04
3b	486	498	494	8	11876	0.47
3c	578	590	584	6	17292	0.15
3d	540	557	551	11	34450	0.52
8	570	585	577	7	–	–
9	693	709	699	6	–	–

[a]Data for **8** and **9** were taken from ref 12.

The thin-film spectra of all of the compounds show a bathochromic shift in their absorption spectra compared to the

DOI: 10.1021/acs.joc.6b01654
J. Org. Chem. 2016, 81, 8485–8494

spectra obtained in solution (Figure 6). We observe broadened absorption peaks, suggesting ground-state $\pi-\pi$ interactions of neighboring molecules in the solid state ("aggregates"). The red shift for **1a** is 20 nm, for **1b** 4 nm, for **1c** 26 nm, for **1d** 13 nm, and for **1e** 10 nm. The absorption maxima shown in Figure 2 are ordered according to the size of the aromatic nucleus, with the diaza- and tetraazapentacene derivatives **1c** and **1e**, respectively, being the ones with the most red-shifted absorption. An interesting optical property is observed when anthracenedione is used instead of naphthalenedione in the syntheses (Figures 4 and 5).

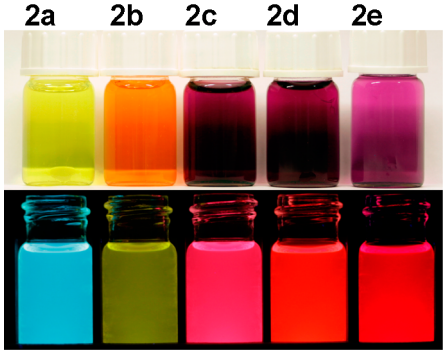

Figure 4. Photographs of **2a–e** (from left to right, respectively) in daylight (top) and under black light with illumination at 365 nm (bottom) in *n*-hexane.

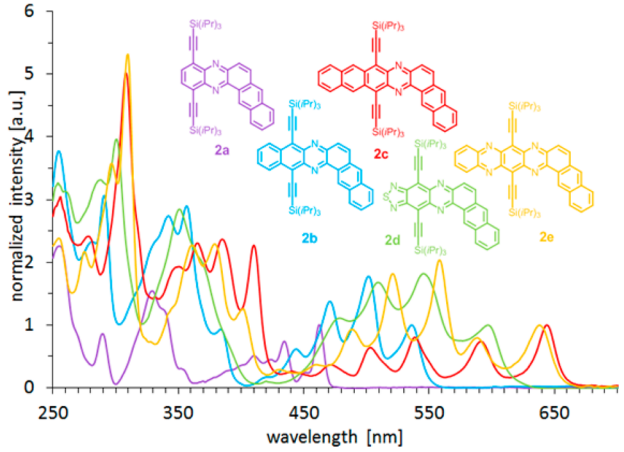

Figure 5. Normalized (lowest-energy maximum) absorption spectra of **2a–e** in *n*-hexane.

While for **2a** the absorption maximum is also red-shifted, the absorption maxima of the other species are up to 28 nm (**2d**) blue-shifted when compared to that of their shorter homologues from group **1a–d** (Table 1). While in solution the UV–vis spectra of **1** and of **2** are fairly similar, in the solid state, an anomaly can be found for compound **2e**; the UV–vis spectrum of **2e** is significantly hypsochromically shifted and broadened in its fine structure (Figure 6). Its behavior is different from that of diaza analogue **2c**, which features a 29 nm red-shifted absorption when going from solution to the solid state.

Figure 7 shows this effect for **2e** in greater detail. It is fairly surprising that the fine structure is nearly lost in the thin-film spectrum compared to the solution spectrum. A tentative explanation for this behavior would be the formation of H-aggregates in the solid state, supported by the odd shape of the absorption maximum and the loss of the other discrete absorption bands.

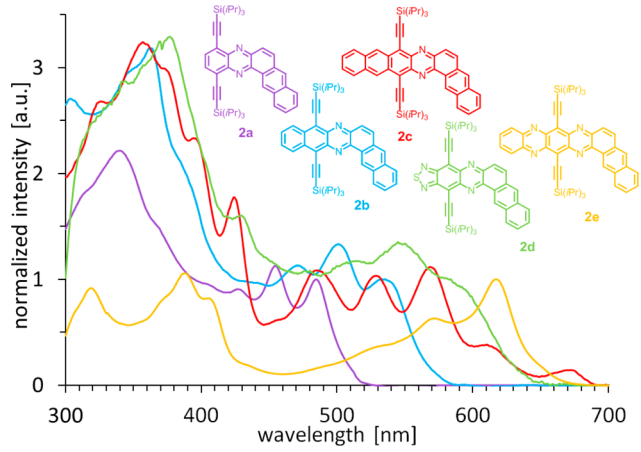

Figure 6. Normalized (lowest-energy maximum) thin-film absorption spectra of **2a–e**. The red shift is 22 nm for **2a**, 29 nm for **2c**, and 5 nm for **2d**. The hypsochromic shift for **2b** (1 nm) and **2e** (20 nm) could be observed.

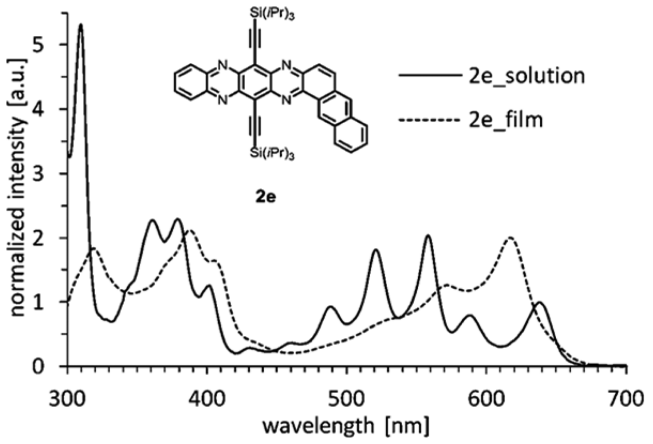

Figure 7. Comparison of the normalized absorption spectra of compound **2e** in film and in *n*-hexane.

H-Aggregates result if two or more molecules stack in a parallel way; for J-aggregates, an end-to-end arrangement is necessary.

The polarization microscope images of the spin-cast thin films of **2c** and **2e** are shown in Figure 8. The images of the films under crossed polarizers indicate small crystallites of **2c**, whereas **2e** appears to be amorphous. The dark field images reveal a dewetting of the glass surface of both thin films, hampering simple device fabrication on glass substrates.

Figures 9 and 10 are instructive and show the packing of **2c** and **2e**, respectively, in a single crystal. In the case of **2c**, there are elements of end-to-end packing mixed with some parallel packing. In **2e**, the parallel packing is more pronounced and the interplanar distances are considerably shorter than in **2c**. The short distances in **2e** support the presence of the proposed H-aggregate species.

In Figure 11, we compare the UV–vis spectra of **1b**, **2b**, and **9** to that of **2e**. The attachment of the bent benzene or the naphthalene unit to the diazaacene leads to a hypsochromic shift in solution. The blue shift is due to the modulation of the electronic properties of the olefin-like ring (circled in Figure 11), which has strong double-bond character. Therefore, this ring does not conjugate with the acene system.

Electrochemistry and Quantum Chemical Calculations. To approximate the ionization potentials and electron affinities,

DOI: 10.1021/acs.joc.6b01654
J. Org. Chem. 2016, 81, 8485–8494

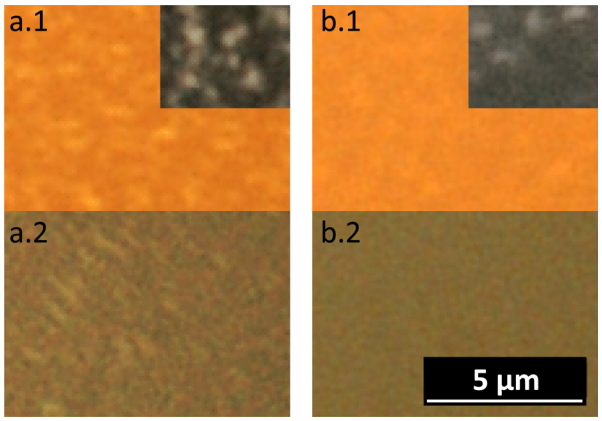

Figure 8. Bright field polarization microscope images of thin films of **2c** (a.1) and **2e** (b.1) spin-cast on glass substrates (insets under dark field illumination) Panels a.2 and b.2 show the corresponding images under cross polarized light.

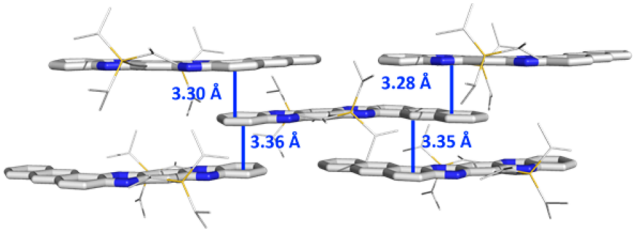

Figure 9. Different distances of neighboring molecules within the packing of compund **2c**.

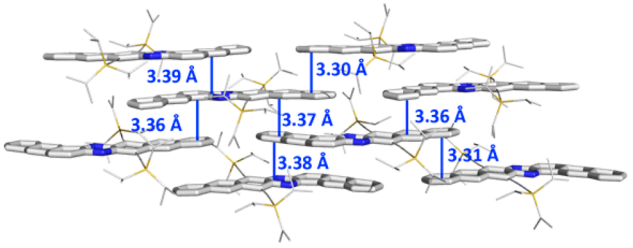

Figure 10. Different distances of neighboring molecules within the packing of compound **2e**.

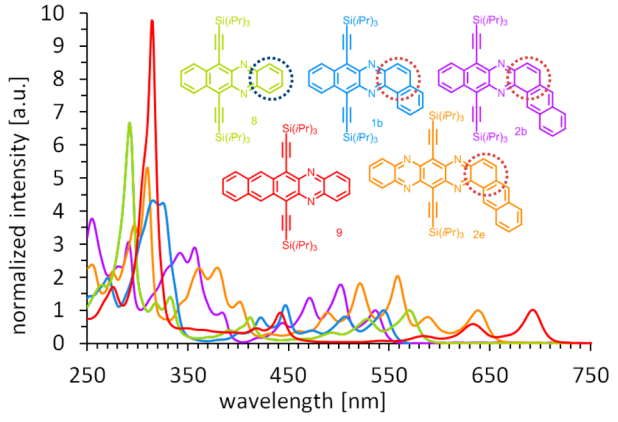

Figure 11. Comparison of the normalized (lowest-energy maximum) absorption spectra of compounds **8**, **9**, **1b**, **1e**, and **2b** in *n*-hexane.

we performed cyclic voltammetry (CV) measurements with ferrocene as the internal reference. **1a**−**3d** display one pseudoreversible reduction peak, $E_{(0/-)}$, and no oxidation peak (Table 2; also see the Supporting Information). All calculated and measured LUMO and HOMO levels together with the gaps are listed in Table 2.

Table 2. Experimental and Calculated (gas-phase) Properties of 1a−e, 2a−e, 3a−d, 8, and TIPS-TAP

compd	$E_{(0/-)}$ (V)[a]	$E_{\text{LUMO CV}}$ (eV)[b]	$E_{\text{gap UV}}$ (eV)[c]	$E_{\text{HOMO DFT}}$ (eV)[d]	$E_{\text{LUMO DFT}}$ (eV)[e]	$E_{\text{g DFT}}$ (eV)[e]
TIPS-TAP	–	−3.99	1.73	−5.78	−3.84	1.94
1a	−1.70	−3.10	2.78	−5.95	−2.95	3.00
1b	−1.49	−3.31	2.22	−5.40	−3.21	2.19
1c	−1.26	−3.54	1.85	−5.24	−3.37	1.87
1d	−0.92	−3.88	1.97	−5.74	−3.73	2.01
1e	−0.81	−3.99	1.86	−5.57	−3.71	1.86
2a	−1.36	−3.45	2.63	−5.92	−2.88	3.04
2b	−1.40	−3.40	2.22	−5.54	−3.15	2.39
2c	−1.20	−3.60	1.85	−5.24	−3.36	1.89
2d	−1.00	−3.81	2.05	−5.73	−3.66	2.07
2e	−1.03	−3.77	1.89	−5.56	−3.66	1.90
3a	−2.18	−2.62	3.05	−5.98	−2.67	3.31
3b	−2.85	−1.95	2.49	−5.58	−2.94	2.64
3c	−1.48	−3.32	1.97	−5.29	−3.12	2.17
3d	−1.33	−3.47	2.23	−5.81	−3.50	2.30
8	–	−3.87	2.12	−5.54	−3.50	1.79
9	–	−4.05	1.75	−5.25	−3.35	1.75

[a]First reduction potentials measured by cyclic voltammetry (CV) in dichlormethane with Bu_4NPF_6 as the electrolyte against Fc/Fc^+ as an internal standard (−4.80 eV) at 0.2 mV/s. [b]$E_{\text{HOMO}} = E_{\text{LUMO CV}} - E_{\text{gap UV}}$. [c]Calculated from CV measurements [$E_{\text{LUMO CV}} = -4.80$ eV − $E_{(0/-)}$]. [d]Calculated from λ_{onset} in hexane. [e]Obtained from quantum chemical calculations with TURBOMOLE B3LYP/def2-TZVP//Gaussian09 B3LYP/6-311++G**.

From quantum chemical calculations on **2a**−**d** (Figure 12) we learn that only for **2a** are HOMO and LUMO fully delocalized.

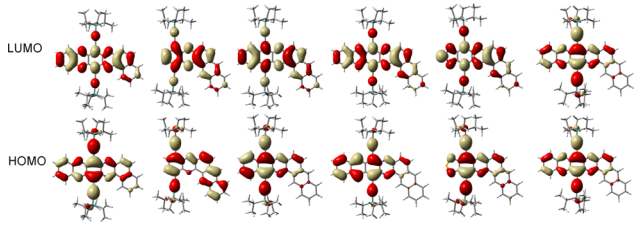

Figure 12. Quantum chemical calculations (TURBOMOLE B3LYP/def2 TZVP//Gaussian 09 B3LYP/6-311++G**) of the FMOs for compounds **1e** and **2a**−**e** (from left to right, respectively). The FMOs of **1a**−**d** are shown in ref 1.

For all of the other members of the group, the frontier molecular orbitals are localized on the benzoquinoxaline part of the molecules. The phenanthrenic addition of the bent naphthalene nucleus in series **2** has an only weak effect on the absorption properties; the slight observed and calculated blue shift (HOMO−LUMO gap and UV−vis spectra) is due to a stabilization of the HOMO and/or a destabilization of the LUMO.

Figure 13 demonstrates the hypsochromic shift upon addition of the phenanthrene-like unit but also the appearance of further absorption bands. In **2e**, where we now have both, a pentacene system but also an added bent naphthalene system, the absorptions around 550 nm are new and not part of the absorption spectrum of TIPS-TAP **8**. The increased absorptive

DOI: 10.1021/acs.joc.6b01654
J. Org. Chem. 2016, 81, 8485−8494

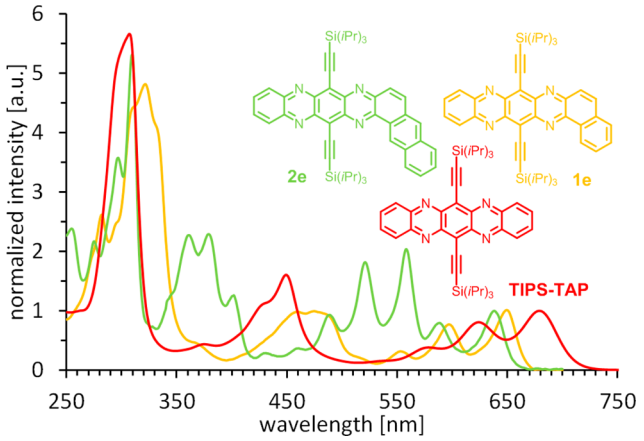

Figure 13. Normalized (lowest-energy maximum) absorption spectra of TIPS-TAP, **1e**, and **2e** in *n*-hexane.

silhouette of the materials such as **2e** might make them useful as absorbers in OPV-type applications.

In the following, we examine compounds **3** with a diazafluorene motif. Figure 14 shows the absorption and emission of **3a**–**d**

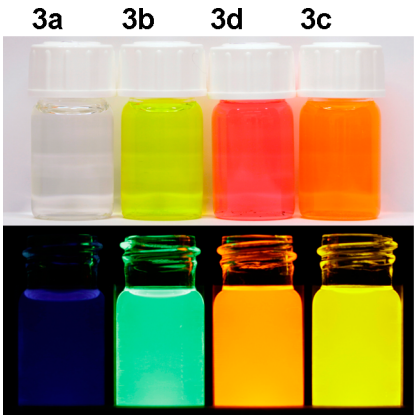

Figure 14. Photographs of **3a**, **3b**, **3d**, and **3c** (from left to right, respectively) in daylight (top) and in *n*-hexane under black light with illumination at 365 nm (bottom).

under daylight and illumination at 365 nm. Figure 15 shows the solution-state absorption spectra of compounds **3** and as a comparison compound **8**. Here the added benzene ring leads to a

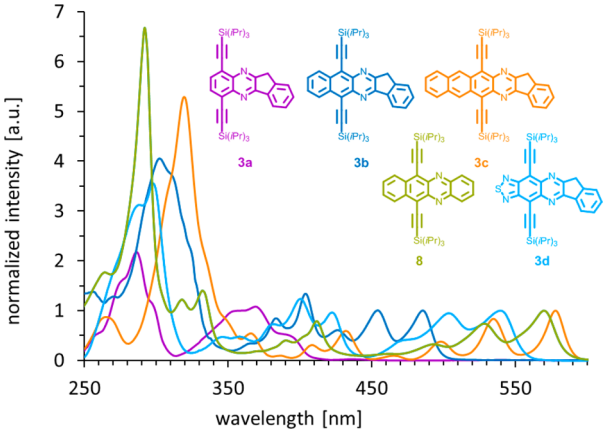

Figure 15. Normalized (lowest-energy maximum) absorption spectra of **3a**–**d** and **8** in *n*-hexane.

small bathochromic shift of the absorption spectra of the compounds.[13] **3b**–**d** show the typical finger structure of the *N*-heteroacenes. The electronic interaction of the benzene ring with the heteroacenes is weak despite the planarity of the systems.

In the solid state, the UV spectra of compounds **3** are unstructured and show absorption tails that range up to 650 nm (**3c**). The shape of the curves points toward microcrystalline films or precipitation on the glass surface (Figure 16).

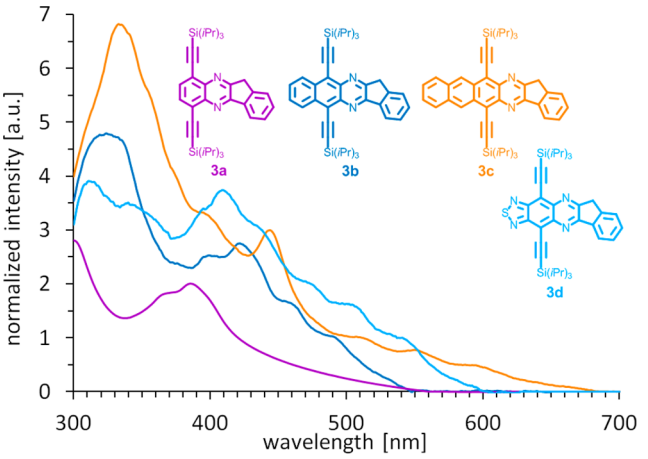

Figure 16. Normalized (lowest-energy maximum) thin-film absorption spectra of **3a**–**d**. The red shift is 18 nm for **3a**, 6 nm for **3b**, 9 nm for **3c**, and 5 nm for **3d**.

The quantum chemical calculations (Figure 17) explain the electronic situation of these systems. The LUMO is extended

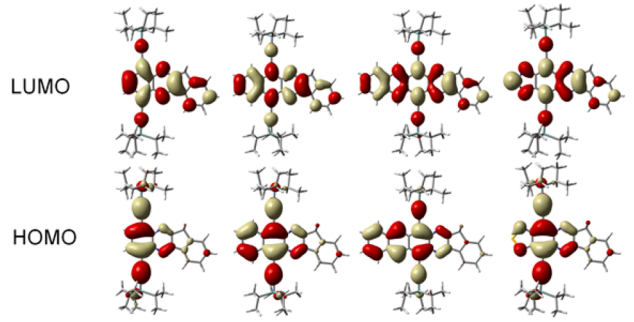

Figure 17. Quantum chemical calculations (TURBOMOLE B3LYP/def2-TZVP//Gaussian09 B3LYP/6-311++G**) of the FMOs for compounds **3a**–**d** (left to right, respectively).

over the whole molecular perimeter (with the exception of the sp_3 methylene group), but the HOMO coefficients are mostly localized on the azaacene unit.

Solid-State Structures. Of further interest are the solid-state structures of the compounds. An overview of different crystalline specimens is depicted in Figure 18, while the structures of **3a** and **3c** can be taken from the Supporting Information. The crystal structures of the *N*-heteroarenes display different packing motifs. **1b** crystallizes in polymorphs **1b i** and **1b ii**. While the smaller *N*-heteroarenes **1a**, **3a**, and **3b** are arranged as pairs, only the slightly larger arenes **1b i** and **2b** form one-dimensional (1D) stacks, which are flipped with respect to each other. All compounds with a thiadiazole motif are packed as 1D, parallel stacks, resulting from alternating head-to-head dimerization of the thiadiazole moiety. This effect is expected and has already been

DOI: 10.1021/acs.joc.6b01654
J. Org. Chem. 2016, 81, 8485–8494

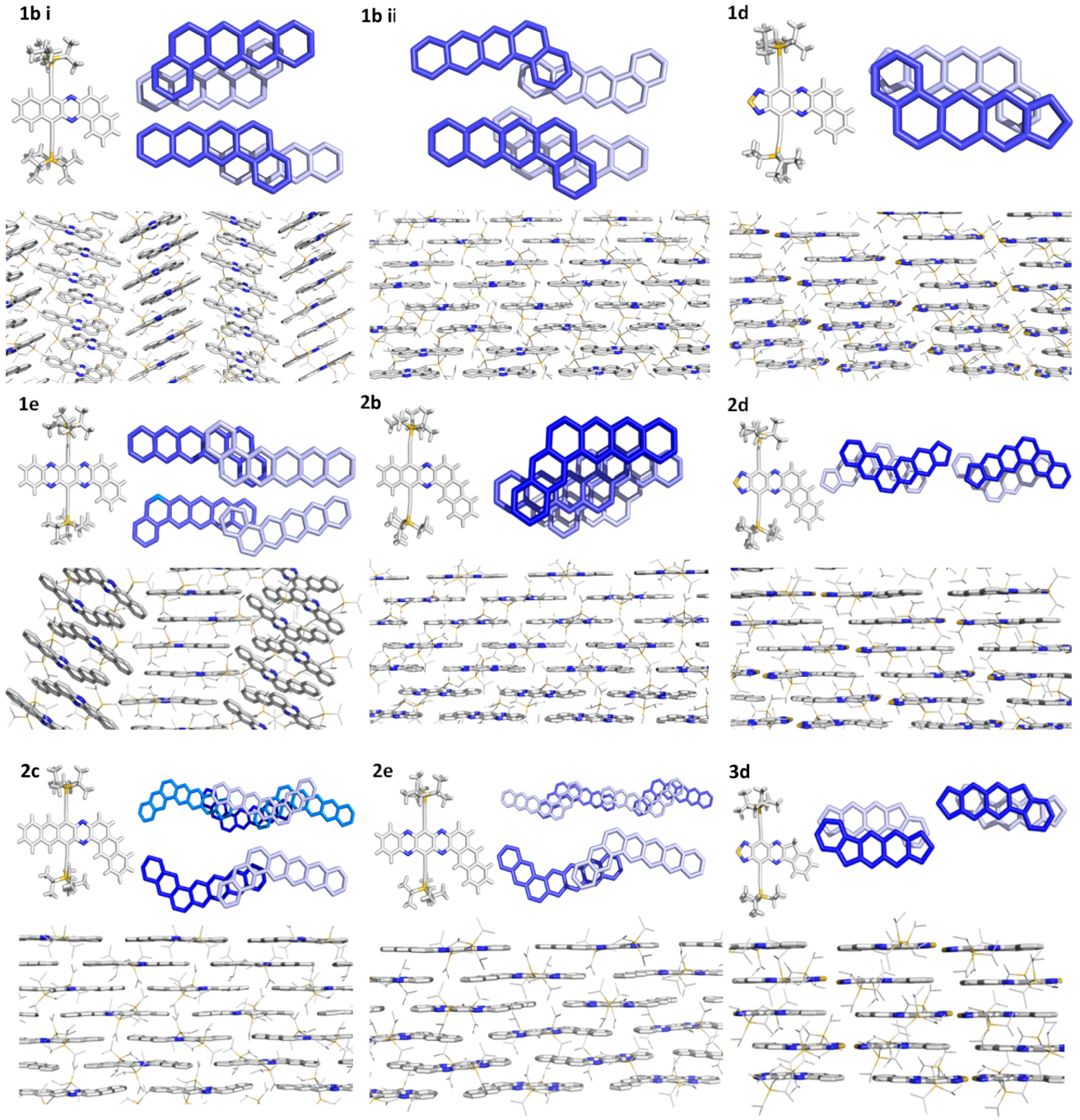

Figure 18. Examples of solid-state structures, viewed along the stack, for the visualization of overlap and packing of compounds **1b**, **1d**, **1e**, **2b**–**e**, and **3d**. **1b** has two different polymorphs: **1b i** as parallel stacks and **1b ii** as a brick-wall motif. The structures of **1b** and **1d** are from ref 1.

described.[14] With an increase in the size of the linear part, the morphology of all larger bent *N*-heteroarenes **1b i**, **1e**, **2c**, and **2e** changes into a brick-wall motif. A hallmark of all crystalline specimens of the bent *N*-heteroarenes is the inverted overlap of the phenanthrenic motif of the molecule. For every structure, a variety of different overlaps is possible, from a "short" overlap to a "long" overlap of the linear and bent parts. As an example, the morphology of **1e** has up to six different overlaps; representative overlaps are shown in Figure 18.

For the singly and doubly annulated compounds **1a**–**c**, **1e**, and **2a**–**e**, the parallel pairs are positioned in such a way that the phenanthrene units stack on top of each other and the distance between the linear parts is fairly small, and the effective overlap of the parallel molecules is reduced. The packing behavior of the compounds of series **3** is comparable to that of the singly annulated derivatives, and within the motif, the CH_2 group of the five-membered rings points outward in opposite directions.

The observed packing patterns have different neighboring molecule distances. This results from the slightly twisted planar molecular structure, caused by the steric repulsion of the bent rest and the TIPS groups. Examples for the different distances of neighboring molecules are shown in Figures 9 and 10, and an overview of all measured distances is given in Table 3. The brick-wall motif packing suggests that these materials might be useful for organic electronics as ambipolar charge transport materials.

DOI: 10.1021/acs.joc.6b01654
J. Org. Chem. 2016, 81, 8485–8494

Table 3. Distances between Neighboring Molecules within the Solid State of 1a, 1b i, 1b ii, 1d, 1e, 2a−e, 3a, 3b, and 3d

	1a	1b i	1b ii	1d	1e	2a	2b	2c	2d	2e	3a	3b	3d
distance (Å)	3.38	3.40−3.40	3.31−3.33	3.42−3.40	3.28−3.35	3.41−3.52	3.42−3.53	3.30−3.39	3.31−3.43	3.28−3.36	3.38−3.44	3.40	3.4−3.53

CONCLUSION

Condensation reactions of the five privileged modules, **7a−e**, with 1,2-naphthalenedione and 1,2-anthracenedione as well as with 1*H*-indene-1,2(3*H*)-dione yield bent *N*-heteroarenes in good to excellent yields. The condensation products, phenanthrene- and fluorene-type *N*-heteropolycycles, are stable, crystalline materials. In the case of **1e** and **2e**, the *N*,*N*′-dihydro compound forms first, which is oxidized by MnO_2 to the desired target. All *N*-heteroarenes could be fully characterized and mostly investigated by single-crystal X-ray analysis.

The attachment of a phenanthrene-type unit to the azaacenes leads, in most cases, to a hypsochromic shift in the solution spectra, as the phenanthrene-type central benzene ring is not available for optimal resonance stabilization of either of the two acene parts that it connects.

EXPERIMENTAL SECTION

All reagents and solvents were obtained from commercial suppliers and used without further purification. For chromatography, the 40−60 °C petrol ether fraction was used. Air- and moisture-sensitive materials were prepared in flame-dried flasks under an atmosphere of nitrogen by using Schlenk techniques. For column chromatography purifications, manual column chromatography (SiO_2, grain size of 0.04−0.063 mm) was used. Polarized microscopy was performed on an optical microscope fitted with cross polarizers and integrated digital imaging. ^{1}H (^{13}C) NMR spectra were recorded on 300 MHz (75 MHz), 400 MHz (100 MHz), 500 MHz (125 MHz), or 600 MHz (150 MHz) spectrometers. The ^{13}C NMR signal structure was analyzed by DEPT and is described as follows: +, primary or tertiary C atom (positive signal); −, secondary C atom (negative signal); Cq, quaternary C atom (no signal). Chemical shifts (δ) are reported in parts per million relative to traces of ^{1}H-labeled solvent in the corresponding deuterated solvent. Mass spectra were recorded using high-resolution direct analysis in real time (HR-DART) detected by a magnetic sector and FT-ICR (Fourier transform ion cyclotron resonance) techniques. Infrared (IR) spectra are reported as solid-phase measurements in wavenumbers (inverse centimeters). Computational studies were conducted using DFT calculations. Geometry optimization was performed at the BP-86/def2-TZVP level. Using this geometry, the absolute energy and FMO energies were assigned via a single-point approach by employing B3LYP/6-311++G**. Thin films were prepared by spin coating a 10 mg/mL solution of the respective substance in dichloromethane on glass slides performed at a speed of 1500 rpm and an acceleration of 1500 rpm/s for 32 s. Pictures were taken under daylight or 365 nm illumination. Quantum yields (Φ) were obtained by the absolute method described in ref 15 using an Ulbricht sphere.[15] The given Φ values for solutions in *n*-hexane are average values of three independent measurements for solutions.

Syntheses. 8,11-Bis[(triisopropylsilyl)ethynyl]benzo[*a*]phenazine (**1a**), 8,13-bis[(triisopropylsilyl)ethynyl]dibenzo[*a*,*i*]phenazine (**1b**), 8,15-bis[(triisopropylsilyl)ethynyl]benzo[*a*]naphtho[2,3-*i*]phenazine (**1c**), 8,12-bis[(triisopropylsilyl)ethynyl]benzo[*a*][1,2,5]thiadiazolo[3,4-*i*]phenazine (**1d**), 3,6-bis[(triisopropylsilyl)ethynyl]benzene-1,2-diamine (**7a**), 1,4-bis[(triisopropylsilyl)ethynyl]naphthalene-2,3-diamine (**7b**), 1,4-bis[(triisopropylsilyl)ethynyl]anthracene-2,3-diamine (**7c**), 4,7-bis[(triisopropylsilyl)ethynyl]benzo[*c*][1,2,5]thiadiazole-5,6-diamine (**7d**), 1,4-bis[(triisopropylsilyl)ethynyl]phenazine-2,3-diamine (**7e**), and anthracene-1,2-dione (**4**) were synthesized according to literature procedures.[1,11,16]

General Procedure (GP). A solution of the *o*-diketone (1.05 equiv) and the *o*-diamine (1.00 equiv) in a 1/1 mixture of dichloromethane and acetic acid was prepared in a round-bottom flask fitted with a condenser. The solution was heated to reflux for 4 h at 80 °C while being stirred. The mixture was cooled to room temperature and carefully diluted with a saturated aqueous solution of sodium hydrogen carbonate (10 mL). The phases were separated, and the aqueous layer was extracted with dichloromethane (3 × 20 mL). The combined organic phases were washed with water (10 mL) followed by brine (10 mL) and then dried over magnesium sulfate. After filtration, the solvent was evaporated, and the crude solid was purified by column chromatography (silicon dioxide, 10/1 petroleum ether/dichloromethane) and crystallized (10/1 ethanol/dichloromethane).

8,15-Bis[(triisopropylsilyl)ethynyl]benzo[*a*]quinoxalino[2,3-*i*]phenazine (1e). The GP was applied to **6** (20.4 mg, 129 μmol, 1.00 equiv) and **7e** (70.0 mg, 123 μmol, 1.05 equiv) in dichloromethane (2 mL) and acetic acid (2 mL). Further purification was achieved by flash column chromatography. This mixture was treated with MnO_2 (150 mg) in dichloromethane (3.00 mL) and stirred for 20 s at room temperature. MnO_2 was removed by filtration through a plug of Celite and the solvent removed under reduced pressure. Flash column chromatography and crystallization (10/1 ethanol/dichloromethane, 10 mL) yielded a dark green crystalline solid. Yield: 46.7 mg, 67.4 μmol, 55%. R_f = 0.55 [SiO_2, 5/1 (v/v) petroleum ether/dichloromethane]. Mp: ≥322 °C dec. ^{1}H NMR ($CDCl_3$, 600.24 MHz): δ 9.57−9.58 (d, 1H), 8.26−8.30 (m, 2H), 7.97−7.99 (d, 1H), 7.86−7.90 (m, 4H), 7.77−7.83 (m, 2H), 1.42−1.43 (m, 21H), 1.38−1.40 (m, 21H). ^{13}C NMR ($CDCl_3$, 150.93 MHz): δ 146.4 (Cq), 145.0 (Cq), 144.9 (Cq), 142.9 (Cq), 142.7 (Cq), 141.7 (Cq), 135.8 (+), 133.8 (Cq), 131.8 (+), 131.2 (+), 131.2 (+), 131.2 (Cq), 130.5 (+), 130.5 (+), 128.6 (+), 128.4 (+), 127.9 (+), 126.9 (+), 122.6 (Cq), 122.4 (Cq), 111.5 (Cq), 110.9 (Cq), 102.8 (Cq), 102.7 (Cq), 102.5 (Cq), 19.0 (+), 19.0 (+), 11.8 (+), 11.7 (+). IR: $\tilde{\nu}$ 2940, 2890, 2862, 2362, 1457, 1382, 1325, 1178, 1064 1023, 994, 880, 746, 673, 595, 544, 673, 583, 471 cm^{-1}. HRMS (direct analysis in real time, DART$^+$): $[M + H]^+$ calcd for $C_{44}H_{53}N_4Si_2$ *m*/*z* 693.3803, found *m*/*z* 693.3829 (correct isotope distribution). Elemental analysis calcd (%) for $C_{44}H_{52}N_4Si_2$: C, 76.15; H, 7.56; N, 8.08. Found: C, 75.66; H, 7.60; N, 8.16. Crystal data: blue crystal (plate), dimensions of 0.210 mm × 0.110 mm × 0.040 mm, triclinic crystal system, space group $P\bar{1}$, Z = 4, a = 14.2395(14) Å, b = 17.3295(17) Å, c = 18.5476(18) Å, α = 74.000(3)°, β = 68.894(3)°, γ = 76.175(3)°, V = 4054.3(7) Å^3, μ = 1.135 g/cm^3, T = 200(2) K, Θ_{max} = 20.492°, 27967 reflections measured, 8021 unique [R(int) = 0.0639], 4297 observed [$I > 2\sigma(I)$], hydrogen atoms treated using appropriate riding models, goodness of fit of 1.60 for observed reflections, final residual values $R_1(F)$ = 0.119 and $wR(F^2)$ = 0.285 for observed reflections, residual electron density of −0.32 to 0.76 e Å^{-3}.

1,4-Bis[(triisopropylsilyl)ethynyl]naphtho[2,3-*a*]phenazine (2a). The GP was applied to **7a** (50.0 mg, 107 μmol, 1.05 equiv) and **4** (21.2 mg, 102 μmol, 1.00 equiv) in dichloromethane (4 mL) and acetic acid (4 mL). Flash column chromatography and crystallization (10/1 ethanol/dichloromethane, 20 mL) yielded a yellow crystalline solid. Yield: 34.6 mg, 53.0 μmol, 52%. R_f = 0.65 [SiO_2, 10/1 (v/v) petroleum ether/ethyl acetate]. Mp: 158−159 °C. ^{1}H NMR ($CDCl_3$, 400.33 MHz): δ 9.98 (s, 1H), 8.35 (s, 1H), 8.16−8.24 (m, 1H), 7.93−8.12 (m, 4H), 7.81 (m, 1H), 7.64−7.69 (m, 2H), 1.33−129 (m, 42H). ^{13}C NMR ($CDCl_3$, 100.67 MHz): δ 145.1 (Cq), 144.1 (Cq), 143.1 (Cq), 141.6 (Cq), 134.6 (+), 133.9 (Cq), 133.7 (+), 133.0 (+), 132.5 (Cq), 131.1 (Cq), 129.1 (+), 129.0 (Cq), 128.2 (+), 127.7 (+), 127.5 (+), 127.3 (+), 127.3 (+), 126.8 (+), 126.4 (+), 124.0 (Cq), 104.1 (Cq), 103.8 (Cq), 100.3 (Cq), 99.5 (Cq), 19.0 (+), 18.8 (+), 11.7 (+), 11.6 (+). IR: $\tilde{\nu}$ 2940, 2862, 2150, 1458, 883, 792, 738, 661, 580, 472 cm^{-1}. HRMS (direct analysis in real time, DART$^+$): $[M + H]^+$ calcd for $C_{42}H_{53}N_2Si_2$ *m*/*z* 641.3742, found *m*/*z* 641.3750 (correct isotope distribution). Elemental analysis calcd (%) for $C_{42}H_{52}N_2Si_2$: C, 78.69; H, 8.18; N, 4.37. Found: C, 78.47; H, 8.19; N, 4.17. Crystal data: yellow crystal (needle), dimensions of 0.190 mm × 0.070 mm × 0.040 mm, triclinic crystal system, space

DOI: 10.1021/acs.joc.6b01654
J. Org. Chem. 2016, 81, 8485−8494

group $P\bar{1}$, $Z = 2$, $a = 7.634(3)$ Å, $b = 14.662(5)$ Å, $c = 17.126(6)$ Å, $\alpha = 87.278(7)°$, $\beta = 84.165(9)°$, $\gamma = 82.636(8)°$, $V = 1890.1(11)$ Å^3, $\mu = 1.126$ g/cm^3, $T = 200(2)$ K, $\Theta_{max} = 17.529°$, 6406 reflections measured, 2325 unique [R(int) = 0.0960], 1462 observed [$I > 2\sigma(I)$], hydrogen atoms treated using appropriate riding models, goodness of fit of 1.11 for observed reflections, final residual values $R_1(F) = 0.072$ and $wR(F^2) = 0.168$ for observed reflections, residual electron density of −0.25 to 0.21 e Å^{-3}.

9,14-Bis[(triisopropylsilyl)ethynyl]benzo[*i*]naphtho[2,3-*a*]-phenazine (2b). The GP was applied to **7b** (100 mg, 193 μmol, 1.05 equiv) and **4** (38.2 mg, 184 μmol, 1.00 equiv) in dichloromethane (7 mL) and acetic acid (7 mL). Flash column chromatography and crystallization (10/1 ethanol/dichloromethane, 30 mL) yielded a red crystalline solid. Yield: 98.9 mg, 143 μmol, 78%. $R_f = 0.75$ [SiO_2, 10/1 (v/v) petroleum ether/ethyl acetate]. Mp: 198−200 °C. ^{1}H NMR ($CDCl_3$, 600.24 MHz): δ 9.99−10.02 (m, 1H), 8.78−8.86 (m, 2H), 8.26−8.39 (m, 2H), 8.19−8.26 (m, 1H), 8.07−8.12 (m, 1H), 7.97−8.02 (m, 1H), 7.66−7.77 (m, 6H), 1.32−1.50 (m, 42H). ^{13}C NMR ($CDCl_3$, 150.93 MHz): δ 146.3 (Cq), 145.1 (Cq), 141.0 (Cq), 139.6 (Cq), 135.6, 135.3, 134.8 (Cq), 134.4 (Cq), 134.1 (Cq), 132.6 (Cq), 131.1 (Cq), 129.2 (+), 129.1 (Cq), 128.3 (+), 128.0 (+), 127.8 (+), 127.7 (+), 127.7 (+), 127.6 (+), 127.5 (+), 127.5 (+), 126.9 (+), 126.9 (Cq), 120.5 (Cq), 120.4 (Cq), 107.3 (Cq), 106.6 (Cq), 103.1 (Cq), 102.8 (Cq), 19.2 (+), 19.0 (+), 11.8 (+), 11.6 (+). IR: $\tilde{\nu}$ 2939, 2862, 2131, 1455, 1383, 1341, 1047, 881, 673, 655 cm^{-1}. HRMS (direct analysis in real time, DART$^+$): [M + H]$^+$ calcd for $C_{46}H_{55}N_2Si_2$ m/z 691.3898, found m/z 691.3888 (correct isotope distribution). Elemental analysis calcd (%) for $C_{46}H_{54}N_2Si_2$: C, 79.94; H, 7.88; N, 4.05. Found: C, 79.60; H, 7.98; N, 3.63. Crystal data: orange crystal (needle), dimensions of 0.560 mm × 0.070 mm × 0.050 mm, monoclinic crystal system, space group $C2/c$, $Z = 8$, $a = 36.272(8)$ Å, $b = 7.4130(16)$ Å, $c = 29.889(7)$ Å, $\alpha = 90°$, $\beta = 94.279(5)°$, $\gamma = 90°$, $V = 8014(3)$ Å^3, $\mu = 1.146$ g/cm^3, $T = 200(2)$ K, $\Theta_{max} = 22.244°$, 18075 reflections measured, 5040 unique [R(int) = 0.0594], 3398 observed [$I > 2\sigma(I)$], hydrogen atoms treated using appropriate riding models, goodness of fit of 1.02 for observed reflections, final residual values $R_1(F) = 0.051$ and $wR(F^2) = 0.113$ for observed reflections, residual electron density of −0.21 to 0.20 e Å^{-3}.

9,16-Bis[(triisopropylsilyl)ethynyl]dinaphtho[2,3-*a*:2′,3′-*i*]-phenazine (2c). The GP was applied to **7c** (40.0 mg, 70.3 μmol, 1.05 equiv) and **4** (14.6 mg, 70. μmol, 1.00 equiv) in dichloromethane (3 mL) and acetic acid (3 mL). Flash column chromatography and crystallization (10/1 ethanol/dichloromethane, 30 mL) yielded a purple crystalline solid. Yield: 19.2 mg, 25.9 μmol, 42%. $R_f = 0.54$ [SiO_2, 10/1 (v/v) petroleum ether/ethyl acetate]. Mp: 297−300 °C. ^{1}H NMR ($CDCl_3$, 400.33 MHz): δ 9.91 (s, 1H), 8.25 (s, 1H), 8.14−8.20 (m, 1H), 8.03−8.10 (m, 1H), 7.97 (d, $J = 9.4$ Hz, 1H), 7.63−7.73 (m, 4H), 1.38−1.48 (m, 22H), 1.24−1.38 (m, 27H). ^{13}C NMR ($CDCl_3$, 100.67 MHz): δ 146.8 (Cq), 145.5 (Cq), 140.8 (Cq), 139.5 (Cq), 135.6 (+), 134.3 (Cq), 132.7 (Cq), 132.7 (Cq), 132.2 (Cq), 131.9 (Cq), 131.2 (Cq), 129.3 (+), 129.2 (Cq), 128.7 (+), 128.7 (+), 128.3 (+), 128.2 (+), 127.8 (+), 127.7 (+), 127.2 (+), 127.0 (+), 126.8 (+), 126.6 (+), 126.6 (+), 120.4 (Cq), 120.3 (Cq), 108.4 (Cq), 107.7 (Cq), 103.9 (Cq), 103.6 (Cq), 19.2 (+), 19.0 (+), 11.9 (+), 11.8 (+). IR: $\tilde{\nu}$ 2939, 2861, 2139, 1461, 1370, 1035, 995, 880, 742, 673, 581, 459 cm^{-1}. HRMS (direct analysis in real time, DART$^+$): [M + H]$^+$ calcd for $C_{50}H_{57}N_2Si_2$ m/z 741.4055, found m/z 741.4068 (correct isotope distribution). Crystal data: dark brown crystal (plate), dimensions of 0.190 mm × 0.190 mm × 0.030 mm, triclinic crystal system, space group $P\bar{1}$, $Z = 4$, $a = 13.744(12)$ Å, $b = 17.701(15)$ Å, $c = 19.206(16)$ Å, $\alpha = 104.207(19)°$, $\beta = 90.814(17)°$, $\gamma = 97.893(19)°$, $V = 4481(7)$ Å^3, $\mu = 1.102$ g/cm^3, $T = 200(2)$ K, $\Theta_{max} = 16.195°$, 15536 reflections measured, 4469 unique [R(int) = 0.1490], 2617 observed [$I > 2\sigma(I)$], hydrogen atoms treated using appropriate riding models, goodness of fit of 1.13 for observed reflections, final residual values $R_1(F) = 0.232$ and $wR(F^2) = 0.518$ for observed reflections, residual electron density of −0.49 to 0.64 e Å^{-3}.

9,13-Bis[(triisopropylsilyl)ethynyl]naphtho[2,3-*a*][1,2,5]-thiadiazolo[3,4-*i*]phenazine (2d). The GP was applied to **7d** (100 mg, 190 μmol, 1.05 equiv) and **4** (37.6 mg, 181 μmol, 1.00 equiv) in dichloromethane (6 mL) and acetic acid (6 mL). Flash column chromatography and crystallization (10/1 ethanol/dichloromethane, 30 mL) yielded a purple crystalline solid. Yield: 59.39 mg, 84.4 μmol, 70%. $R_f = 0.65$ [SiO_2, 10/1 (v/v) petroleum ether/ethyl acetate]. Mp: ≥254 °C dec. ^{1}H NMR ($CDCl_3$, 600.24 MHz): δ 9.91 (s, 1H), 8.25 (s, 1H), 8.14−8.20 (m, 1H), 8.03−8.10 (m, 1H), 7.97 (m, 1H), 7.63−7.73 (m, 4H), 1.24−1.48 (m, 42H). ^{13}C NMR ($CDCl_3$, 150.93 MHz): δ 154.7 (Cq), 154.2 (Cq), 147.5 (Cq), 146.3 (Cq), 142.9 (Cq), 141.5 (Cq), 136.8 (+), 134.4 (Cq), 132.7 (Cq), 131.0 (Cq), 129.4 (+), 128.6 (Cq), 128.4 (+), 128.2 (+), 128.1 (+), 127.8 (+), 127.7 (+), 127.3 (+), 114.0 (Cq), 113.9 (Cq), 110.2 (Cq), 109.5 (Cq), 101.8 (Cq), 101.6 (Cq), 19.1 (+), 18.9 (+), 11.7 (+), 11.6 (+). IR: $\tilde{\nu}$ 2940, 2889, 2862, 2131, 1544, 1456, 1365, 1018, 881, 736, 671, 472 cm^{-1}. HRMS (direct analysis in real time, DART$^+$): [M + H]$^+$ calcd for $C_{42}H_{51}N_4SSi_2$ m/z 699.3367, found m/z 699.3368 (correct isotope distribution). Crystal data: red crystal (plate), dimensions of 0.280 mm × 0.150 mm × 0.040 mm, triclinic crystal system, space group $P\bar{1}$, $Z = 2$, $a = 8.241(3)$ Å, $b = 14.201(5)$ Å, $c = 17.856(6)$ Å, $\alpha = 68.710(8)°$, $\beta = 80.696(8)°$, $\gamma = 74.394(8)°$, $V = 1870.6(11)$ Å^3, $\mu = 1.241$ g/cm^3, $T = 100(2)$ K, $\Theta_{max} = 22.379°$, 10985 reflections measured, 4750 unique [R(int) = 0.0988], 2589 observed [$I > 2\sigma(I)$], hydrogen atoms treated using appropriate riding models, goodness of fit of 1.05 for observed reflections, final residual values $R_1(F) = 0.084$ and $wR(F^2) = 0.152$ for observed reflections, residual electron density of −0.35 to 0.28 e Å^{-3}.

9,16-Bis[(triisopropylsilyl)ethynyl]naphtho[2,3-*a*]-quinoxalino[2,3-*i*]phenazine (2e). The GP was applied to **4** (17.4 mg, 36.7 μmol, 1.00 equiv) and **7e** (50.0 mg, 87.6 μmol, 1.05 equiv) in dichloromethane (2 mL) and acetic acid (2 mL). Further purification was achieved by flash column chromatography. This mixture was treated with MnO_2 (150 mg) in dichloromethane (3.00 mL) and stirred for 20 s at room temperature. MnO_2 was removed by filtration through a plug of Celite and the solvent removed under reduced pressure. Flash column chromatography and crystallization [SiO_2, 10/1 (v/v) petroleum ether/ethyl acetate] yielded a purple crystalline solid. Yield: 21.0 mg, 28.4 μmol, 34%. $R_f = 0.55$ [SiO_2, 5/1 (v/v) petroleum ether/ethyl acetate]. Mp: ≥304 °C dec. ^{1}H NMR ($CDCl_3$, 600.24 MHz): δ 10.00 (s, 1H), 8.27−8.31 (m, 3H), 8.18−8.20 (m, 1H), 8.07−8.09 (m, 1H), 8.00−7.99 (d, 1H), 7.87−7.89 (m, 2H), 7.74−7.73 (d, 1H), 7.68−7.70 (m, 2H), 1.49 (m, 21H), 1.38−1.41 (m, 21H). ^{13}C NMR ($CDCl_3$, 150.06 MHz): δ 147.6 (Cq), 146.3 (Cq), 144.9 (Cq), 144.9 (Cq), 143.0 (Cq), 143.0 (Cq), 142.7 (Cq), 141.7 (Cq), 136.8 (+), 134.4 (Cq), 132.7 (Cq), 131.6 (+), 131.6 (+), 131.0 (Cq), 130.5 (+), 130.4 (+), 129.5 (+), 128.8 (Cq), 128.4 (+), 128.2 (+), 128.0 (+), 128.0 (+), 127.9 (+), 127.3 (+), 122.1 (Cq), 111.0 (Cq), 110.3 (Cq), 102.9 (Cq), 102.6 (Cq), 19.2 (+), 19.0 (+), 11.9 (+), 11.7 (+). IR: $\tilde{\nu}$ 3058, 2939, 2889, 2861, 2145, 1593, 1505, 1454, 1381, 1312, 1247, 1191, 1051, 1021, 993, 881, 742, 673, 583, 471 cm^{-1}. HRMS (direct analysis in real time, DART$^+$): [M + 3H]$^+$ calcd for $C_{48}H_{57}N_4Si_2$ m/z 745.4116, found m/z 745.4127 (correct isotope distribution). Crystal data: violet crystal (plate), dimensions of 0.170 mm × 0.110 mm × 0.060 mm, monoclinic crystal system, space group $P2_1/c$, $Z = 4$, $a = 17.830(2)$ Å, $b = 19.068(2)$ Å, $c = 13.5277(16)$ Å, $\alpha = 90°$, $\beta = 92.340(4)°$, $\gamma = 90°$, $V = 4595.4(10)$ Å^3, $\mu = 1.136$ g/cm^3, $T = 200(2)$ K, $\Theta_{max} = 19.446°$, 18672 reflections measured, 3946 unique [R(int) = 0.0852], 2143 observed [$I > 2\sigma(I)$], hydrogen atoms treated using appropriate riding models, goodness of fit of 1.01 for observed reflections, final residual values $R_1(F) = 0.068$ and $wR(F^2) = 0.169$ for observed reflections, residual electron density of −0.21 to 0.24 e Å^{-3}.

6,9-Bis[(triisopropylsilyl)ethynyl]-11*H*-indeno[1,2-*b*]-quinoxaline (3a). The GP was applied to **7a** (100 mg, 213 μmol, 1.05 equiv) and **5** (28.7 mg, 203 μmol, 1.00 equiv) in dichloromethane (7 mL) and acetic acid (7 mL). Flash column chromatography and crystallization (10/1 ethanol/dichloromethane, 40 mL) yielded a weak yellow crystalline solid. Yield: 83.7 mg, 115 μmol, 71%. $R_f = 0.76$ [SiO_2, 10/1 (v/v) petroleum ether/ethyl acetate]. Mp: 196−197 °C. ^{1}H NMR ($CDCl_3$, 600.24 MHz): δ 8.20−8.24 (m, 1H), 7.79−7.86 (m, 2H), 7.65 (m, 1H), 7.51−7.56 (m, 2H), 4.17 (s, 2H), 1.23−1.29 (m, 42H). ^{13}C NMR ($CDCl_3$, 150.93 MHz): δ 160.4 (Cq), 155.2 (Cq), 144.2 (Cq), 143.2 (Cq), 142.2 (Cq), 138.4 (Cq), 132.9 (+), 132.4 (+), 131.4 (+), 128.2 (+), 125.9 (+), 124.1 (Cq), 124.0 (Cq), 123.3 (+), 113.8 (+), 104.1 (Cq), 104.1 (Cq), 99.7 (Cq), 99.5 (Cq), 36.2 (−), 19.0 (+), 11.7 (+). IR: $\tilde{\nu}$ 2939, 2887, 2861, 2147, 1460, 1379, 996, 882, 797, 670, 594, 578, 430 cm^{-1}. HRMS (direct analysis in real time, DART$^+$): [M + H]$^+$

DOI: 10.1021/acs.joc.6b01654
J. Org. Chem. 2016, 81, 8485−8494

calcd for $C_{37}H_{51}N_2Si_2$ m/z 579.3585, found m/z 579.3585 (correct isotope distribution). Elemental analysis calcd (%) for $C_{37}H_{50}N_2Si_2$: C, 76.76; H, 8.70; N, 4.84. Found: C, 76.57; H, 8.83; N, 4.68. Crystal data: yellow crystal (octahedron), dimensions of 0.390 mm × 0.170 mm × 0.130 mm, monoclinic crystal system, space group $P2_1/c$, Z = 4, a = 8.8801(10) Å, b = 18.143(2) Å, c = 21.186(3) Å, α = 90°, β = 96.813(2)°, γ = 90°, V = 3389.3(7) Å^3, μ = 1.135 g/cm^3, T = 200(2) K, Θ_{max} = 29.188°, 34016 reflections measured, 8932 unique [R(int) = 0.0490], 6654 observed [$I > 2\sigma(I)$], hydrogen atoms treated using appropriate riding models, goodness of fit of 1.04 for observed reflections, final residual values $R_1(F)$ = 0.056 and $wR(F^2)$ = 0.110 for observed reflections, residual electron density of −0.43 to 0.47 e Å^{-3}.

6,11-Bis[(triisopropylsilyl)ethynyl]-13*H*-benzo[*g*]indeno[1,2-*b*]quinoxaline (3b). The GP was applied to **7b** (100 mg, 193 μmol, 1.05 equiv) and **5** (26.8 mg, 184 μmol, 1.00 equiv) in dichloromethane (7 mL) and acetic acid (7 mL). Flash column chromatography and crystallization (10/1 ethanol/dichloromethane, 30 mL) yielded a yellow crystalline solid. Yield: 106 mg, 169 μmol, 92%. R_f = 0.75 [SiO_2, 10/1 (v/v) petroleum ether/ethyl acetate]. Mp: 202−206 °C. ^{1}H NMR ($CDCl_3$, 600.24 MHz): δ 8.77 (m, 2H), 8.28 (m, 1H), 7.64−7.72 (m, 3H), 7.52−7.60 (m, 2H), 4.22 (s, 2H), 1.29−1.38 (m, 42H). ^{13}C NMR ($CDCl_3$, 100.67 MHz): δ 161.0 (Cq), 155.5 (Cq), 144.5 (Cq), 140.9 (Cq), 140.1 (Cq), 138.1 (Cq), 134.0 (Cq), 133.6 (Cq), 131.7 (+), 128.1 (+), 127.6 (+), 127.5 (+), 127.4 (+), 127.3 (+), 125.8 (+), 123.5 (+), 120.6 (Cq), 120.5 (Cq), 106.2 (Cq), 106.1 (Cq), 102.7 (Cq), 102.5 (Cq), 101.2 (+), 36.0 (−), 18.9 (+), 11.6 (+). IR: $\tilde{\nu}$ 2939, 2889, 2862, 2138, 1608, 1461, 1382, 1343, 1239, 1055, 1027, 880, 762, 725, 674, 658, 588, 568, 538, 483, 470 cm^{-1}. HRMS (direct analysis in real time, DART$^+$): [M + H]$^+$ calcd for $C_{41}H_{53}N_2Si_2$ m/z 629.3742, found m/z 629.3734 (correct isotope distribution). Crystal data: yellow crystal (needle), dimensions of 0.620 mm × 0.050 mm × 0.050 mm, monoclinic crystal system, space group $P2_1/n$, Z = 4, a = 17.380(9) Å, b = 8.062(4) Å, c = 27.836(13) Å, α = 90°, β = 104.082(11)°, γ = 90°, V = 3783(3) Å^3, μ = 1.104 g/cm^3, T = 200(2) K, Θ_{max} = 16.769°, 9347 reflections measured, 2113 unique [R(int) = 0.0921], 1344 observed [$I > 2\sigma(I)$], hydrogen atoms treated using appropriate riding models, goodness of fit of 1.04 for observed reflections, final residual values $R_1(F)$ = 0.078 and $wR(F^2)$ = 0.193 for observed reflections, residual electron density of −0.26 to 0.40 e Å^{-3}.

6,13-Bis[(triisopropylsilyl)ethynyl]-15*H*-indeno[1,2-*b*]-naphtho[2,3-*g*]quinoxaline (3c). The GP was applied to **7c** (40.0 mg, 70.3 μmol, 1.05 equiv) and **5** (9.78 mg, 67.0 μmol, 1.00 equiv) in dichloromethane (2 mL) and acetic acid (2 mL). Flash column chromatography and crystallization (10/1 ethanol/dichloromethane, 30 mL) yielded a purple crystalline solid. Yield: 31.0 mg, 45.7 μmol, 68%. R_f = 0.72 [SiO_2, 10/1 (v/v) petroleum ether/ethyl acetate]. Mp: ≥260 °C dec. ^{1}H NMR (THF-d_8, 600.24 MHz): δ 8.66 (d, J = 5.0 Hz, 2H), 7.52 (d, J = 7.2 Hz, 1H), 7.34 (m, 2H), 6.96 (d, J = 7.4 Hz, 1H), 6.76−6.85 (m, 4H), 3.49 (s, 2H), 2.83 (s, 9H), 0.52−0.65 (m, 42H). ^{13}C NMR (THF-d_8, 150.93 MHz): δ 162.9 (Cq), 156.8 (Cq), 146.5 (Cq), 142.0 (Cq), 141.3 (Cq), 139.0 (Cq), 133.7 (Cq), 133.7 (Cq), 133.2 (+), 132.3 (Cq), 131.9 (Cq), 129.4 (+), 129.4 (+), 129.0 (+), 127.7 (+), 127.6 (+), 127.4 (+), 127.3 (+), 127.1 (+), 124.1 (+), 121.4 (Cq), 121.4 (Cq), 107.3 (Cq), 107.1 (Cq), 104.8 (Cq), 104.7 (Cq), 30.8 (−), 19.6 (+), 19.5 (+), 12.8 (+), 12.8 (+). IR: $\tilde{\nu}$ 2921, 2890, 2862, 2143, 1611, 1461, 1342, 1054, 994, 878, 661, 578, 459 cm^{-1}. HRMS (direct analysis in real time, DART$^+$): [M + H]$^+$ calcd for $C_{45}H_{55}N_2Si_2$ m/z 679.3898, found m/z 679.3909 (correct isotope distribution). Elemental analysis calcd (%) for $C_{45}H_{54}N_2Si_2$: C, 79.59; H, 8.02; N, 4.13. Found: C, 79.52; H, 7.87; N, 3.46.

4,12-Bis[(triisopropylsilyl)ethynyl]-10*H*-indeno[1,2-*b*][1,2,5]-thiadiazolo[3,4-*g*]quinoxaline (3d). The GP was applied to **7d** (50.0 mg, 95.0 μmol, 1.05 equiv) and **5** (13.2 mg, 90.4 μmol, 1.00 equiv) in dichloromethane (4 mL) and acetic acid (4 mL). Flash column chromatography and crystallization (10/1 ethanol/dichloromethane, 10 mL) yielded an orange crystalline solid. Yield: 29.4 mg, 46.0 μmol, 52%. R_f = 0.68 [SiO_2, 10/1 (v/v) petroleum ether/ethyl acetate]. Mp: ≥222 °C dec. ^{1}H NMR ($CDCl_3$, 400.33 MHz): δ 8.28 (d, J = 7.3 Hz, 1H), 7.54−7.70 (m, 4H), 4.22 (s, 2H), 1.28−1.35 (m, 42H). ^{13}C NMR ($CDCl_3$, 100.67 MHz): δ 162.4 (Cq), 156.5 (Cq), 154.3 (Cq), 154.0 (Cq), 145.0 (Cq), 143.3 (Cq), 142.4 (Cq), 137.6 (Cq), 132.6 (+), 128.4 (+), 126.0 (+), 123.9 (+), 114.5 (Cq), 114.3 (Cq), 108.8 (Cq), 108.7 (Cq), 101.2 (Cq), 101.1 (Cq), 29.7 (−), 18.8 (+), 11.6 (+). IR: $\tilde{\nu}$ 2922, 2863, 1607, 1463, 1359, 1062, 1008, 883, 723, 676, 592, 512 cm^{-1}. HRMS (direct analysis in real time, DART$^+$): [M + H]$^+$ calcd for $C_{37}H_{49}N_4SSi_2$ m/z 637.3211, found m/z 637.3222 (correct isotope distribution). Crystal data: orange crystal (plate), dimensions of 0.300 mm × 0.180 mm × 0.050 mm, monoclinic crystal system, space group $P2_1/c$, Z = 4, a = 7.369(4) Å, b = 12.752(7) Å, c = 37.432(19) Å, α = 90°, β = 91.497(14)°, γ = 90°, V = 3516(3) Å^3, μ = 1.203 g/cm^3, T = 100(2) K, Θ_{max} = 20.900°, 10761 reflections measured, 3645 unique [R(int) = 0.1310], 2099 observed [$I > 2\sigma(I)$], hydrogen atoms treated using appropriate riding models, goodness of fit of 1.10 for observed reflections, final residual values $R_1(F)$ = 0.147 and $wR(F^2)$ = 0.344 for observed reflections, residual electron density of −0.56 to 0.62 e Å^{-3}.

■ ASSOCIATED CONTENT

Supporting Information

The Supporting Information is available free of charge on the ACS Publications website at DOI: 10.1021/acs.joc.6b01654.

Optical spectra (emission, IR), electrochemical measurements, NMR spectra, and solid-state and crystal structures (PDF)

Coordinates of the computational chemistry calculations (PDF)

Crystallographic data (CIF)

■ AUTHOR INFORMATION

Corresponding Author

*E-mail: uwe.bunz@oci.uni-heidelberg.de.

Notes

The authors declare no competing financial interest.

■ ACKNOWLEDGMENTS

We thank the Deutsche Forschungsgemeinschaft for generous funding (Bu771/7-3).

■ REFERENCES

(1) Hahn, S.; Biegger, P.; Bender, M.; Rominger, F.; Bunz, U. H. F. *Chem. - Eur. J.* **2016**, *22*, 869−873.

(2) (a) Anthony, J. E.; Brooks, J. S.; Eaton, D. L.; Parkin, S. R. *J. Am. Chem. Soc.* **2001**, *123*, 9482−9483. (b) Payne, M. M.; Parkin, S. R.; Anthony, J. E. *J. Am. Chem. Soc.* **2005**, *127*, 8028−8029.

(3) (a) Anthony, J. E. *Chem. Rev.* **2006**, *106*, 5028−5048. (b) Anthony, J. E. *Angew. Chem., Int. Ed.* **2008**, *47*, 452−483.

(4) Scott, L. T. *Angew. Chem., Int. Ed.* **2004**, *43*, 4994−5007.

(5) Weil, T.; Vosch, T.; Hofkens, J.; Peneva, K.; Müllen, K. *Angew. Chem., Int. Ed.* **2010**, *49*, 9068−9093.

(6) Hinsberg, O. *Liebigs Ann. Chem.* **1901**, *319*, 257−286.

(7) Bunz, U. H. F. *Pure Appl. Chem.* **2010**, *82*, 953−968.

(8) Miao, S.; Appleton, A. L.; Berger, N.; Barlow, S.; Marder, S. R.; Hardcastle, K. I.; Bunz, U. H. F. *Chem. - Eur. J.* **2009**, *15*, 4990−4993.

(9) (a) Liang, Z. X.; Tang, Q.; Xu, J. B.; Miao, Q. A. *Adv. Mater.* **2011**, *23*, 1535−1539. (b) Paulus, F.; Engelhart, J.; Hopkinson, P.; Schimpf, C.; Leineweber, A.; Sirringhaus, H.; Vaynzof, Y.; Bunz, U. H. F. *J. Mater. Chem. C* **2016**, *4*, 1194−1200. (c) Paulus, F.; Porz, M.; Schaffroth, M.; Rominger, F.; Leineweber, A.; Vaynzof, Y.; Bunz, U. H. F. *Org. Electron.* **2016**, *33*, 102−109.

(10) (a) Miao. *Synlett* **2012**, *23*, 326−336. (b) Bunz, U. H. F.; Engelhart, J. U.; Lindner, B. D.; Schaffroth, M. *Angew. Chem., Int. Ed.* **2013**, *52*, 3810−3821. (c) Bunz, U. H. F. *Acc. Chem. Res.* **2015**, *48*, 1676−1686. (d) Bunz, U. H. F. *Chem. - Eur. J.* **2009**, *15*, 6780−6789. (e) Bunz, U. H. F.; Engelhart, J. U. *Chem. - Eur. J.* **2016**, *22*, 4680−4689.

(11) (a) Lindner, B. D.; Engelhart, J. U.; Tverskoy, O.; Appleton, A. L.; Rominger, F.; Peters, A.; Himmel, H. J.; Bunz, U. H. F. *Angew. Chem., Int. Ed.* **2011**, *50*, 8588−8591. (b) Engelhart, J. U.; Tverskoy, O.; Bunz, U. H. F. *J. Am. Chem. Soc.* **2014**, *136*, 15166−15169.

(12) Biegger, P.; Stolz, S.; Intorp, S. N.; Zhang, Y.; Engelhart, J. U.; Rominger, F.; Hardcastle, K. I.; Lemmer, U.; Qian, X.; Hamburger, M.; Bunz, U. H. F. *J. Org. Chem.* **2015**, *80*, 582−589.
(13) Appleton, A. L.; Miao, S.; Brombosz, S. M.; Berger, N. J.; Barlow, S.; Marder, S. R.; Lawrence, B. M.; Hardcastle, K. I.; Bunz, U. H. F. *Org. Lett.* **2009**, *11*, 5222−5225.
(14) Lindner, B. D.; Paulus, F.; Appleton, A. L.; Schaffroth, M.; Engelhart, J. U.; Schelkle, K. M.; Tverskoy, O.; Rominger, F.; Hamburger, M.; Bunz, U. H. F. *J. Mater. Chem. C* **2014**, *2*, 9609−9612.
(15) Würth, C.; Grabolle, M.; Pauli, J.; Spieles, M.; Resch-Genger, U. *Nat. Protoc.* **2013**, *8*, 1535.
(16) (a) Lindner, B. D.; Coombs, B. A.; Schaffroth, M.; Engelhart, J. U.; Tverskoy, O.; Rominger, F.; Hamburger, M.; Bunz, U. H. F. *Org. Lett.* **2013**, *15*, 666−669. (b) Miao, S.; Brombosz, S. M.; Schleyer, P. v. R.; Wu, J. I.; Barlow, U. S.; Marder, S. R.; Hardcastle, K. I.; Bunz, U. H. F. *J. Am. Chem. Soc.* **2008**, *130*, 7339−7344. (c) Wu, A.; Duan, Y.; Xu, D.; Penning, T. M.; Harvey, R. G. *Tetrahedron* **2010**, *66*, 2111−2118.

DOI: 10.1021/acs.joc.6b01654
J. Org. Chem. 2016, 81, 8485−8494